





## Article

# Microorganisms Isolated from Saharan Dust Intrusions in the Canary Islands and Processes of Mineral Atmospherogenesis

Azahara Navarro <sup>1</sup>, Ana del Moral <sup>2,\*</sup>, Irene de Pablos <sup>1</sup>, Rafael Delgado <sup>1</sup>, Jesús Párraga <sup>1</sup>, Juan M. Martín-García <sup>1</sup> and Fernando Martínez-Checa <sup>2,3</sup>

<sup>1</sup> Department of Soil Science, University of Granada, 18071 Granada, Spain; mnavarro796@ugr.es (A.N.); irenedepablos@correo.ugr.es (I.d.P.); rdelgado@ugr.es (R.D.); jparraga@ugr.es (J.P.); jmmartingarcia@ugr.es (J.M.M.-G.)

<sup>2</sup> Department of Microbiology, University of Granada, 18071 Granada, Spain; fmchecha@ugr.es

<sup>3</sup> Center for Biomedical Research (CIBM), Institute of Biotechnology, University of Granada, 18071 Granada, Spain

\* Correspondence: admoral@ugr.es

**Abstract:** Global warming due to climate change has increased the frequency of sand and dust storms that affect air quality and ecosystems in general, contributing to air pollution. The Sahara Desert is the most potent emitter of atmospheric dust. The atmosphere is an extreme environment and microorganisms living in the troposphere are exposed to greater ultraviolet radiation, desiccation, low temperatures and nutrient deprivation than in other habitats. The Iberian Peninsula, and specifically the Canary Islands—due to its strategic location—is one of the regions that receive more Saharan dust particles annually, increasing year after year, although culturable microorganisms had previously never been described. In the present work, dust samples were collected from three calima events in the Canary Islands between 2021 and 2022. The sizes, mineralogical compositions and chemical compositions of dust particles were determined by laser diffraction, X-ray diffraction (XRD) and X-ray photoelectron spectroscopy (XPS), respectively. Particle morphology and biological features were also studied by scanning electron microscopy (SEM-EDX) and confocal laser scanning microscopy (CLSM). The mineral–bacteria interactions were described from microscopic observations, which revealed the presence of iberulites and small neofomed kaolinite crystals in association with bacteria. This article defines the term “mineral atmospherogenesis” and its variant, “mineral bioatmospherogenesis”, through microbial interaction. This is the first described case of kaolinite produced through mineral bioatmospherogenesis. The bacterial growth in atmospheric dust was illustrated in SEM images, constituting a novel finding. Twenty-three culturable microorganisms were isolated and identified by 16S rRNA sequencing. Members of the phyla *Pseudomonadota*, *Bacillota* and *Actinomycetota* have been found. Some of these microorganisms, such as *Peribacillus frigoritolerans*, have Plant Growth-Promoting Rhizobacteria (PGPR) properties. Potential human pathogenic bacteria such as *Acinetobacter lwoffii* were also found. The presence of desert dust and iberulites in the Canary Islands, together with transported biological components such as bacteria, could have a significant impact on the ecosystem and human health.

**Keywords:** extremophiles; Saharan dust; iberulite; atmospherogenesis; Canary Islands; calima; biofilm



**Citation:** Navarro, A.; del Moral, A.; de Pablos, I.; Delgado, R.; Párraga, J.; Martín-García, J.M.; Martínez-Checa, F. Microorganisms Isolated from Saharan Dust Intrusions in the Canary Islands and Processes of Mineral Atmospherogenesis. *Appl. Sci.* **2024**, *14*, 1862. <https://doi.org/10.3390/app14051862>

Academic Editor: Paola Grenni

Received: 31 January 2024

Revised: 16 February 2024

Accepted: 22 February 2024

Published: 24 February 2024



**Copyright:** © 2024 by the authors. Licensee MDPI, Basel, Switzerland. This article is an open access article distributed under the terms and conditions of the Creative Commons Attribution (CC BY) license (<https://creativecommons.org/licenses/by/4.0/>).

## 1. Introduction

The amount of dust originating from desert areas and circulating around the planet has increased over the last few decades [1]. Numerous studies on Saharan dust and its consequences have sparked a great interest in dust storms and their influence on ecosystems.

Desert areas and other arid regions constitute the main source of mineral dust particles in the atmosphere [2]. The Sahara Desert is the predominant source of mineral dust globally, which can be subsequently spread southwards (60%) and westwards to the Atlantic Ocean (25%), eastwards to the Middle East (5%) and northwards to Europe (10%) [3,4].

Biological material transported by dust storms deserves special attention. Extreme conditions such as high/low temperatures, high hydrostatic pressures, high salt concentration or high/low pH values define different types of extreme environments, suitable for extremophilic microorganisms [5]. The atmosphere, despite being the largest biome on Earth, remains one of the least understood environments in terms of microbial activity [6]. Due to radiation and temperature changes, it is one of the most extreme environments described so far. Some bacteria, fungi and viruses can survive in the atmosphere despite enduring different environmental stressors [7,8].

Microbes attached to dust particles can be transported through the atmosphere and dispersed in exogenous environments [9–12]. The long-range transport of viable bacteria along with mineral aerosols may represent a pathway for bacteria to colonize new environments and alter the existing diversity in remote terrestrial and aquatic habitats [7,13].

Dust intrusions can be accompanied by a characteristic precipitation known as red rain, dust rain, bloody rain, coloured rain or muddy rain [14,15]. Recently isolated culturable microorganisms and other microbial communities have been described in red rain episodes in the southeast of Spain [16].

A striking phenomenon is the occurrence of corpuscles with 50–200 µm diameters and quasi-spherical morphology, known as iberulites [17]. Iberulites are typically observed during Saharan dust intrusions in the Iberian Peninsula and the Canary Islands. These particles account for atmospheric “giant” aerosols as they have a low density and a porosity about 50%, covering thousands of kilometres and facilitating the intercontinental transport of spore-forming and viable microorganisms either in their external rind or inside them [18].

The Canary Islands, situated between 100 and 500 km off the northwest coast of Africa, are often affected by Saharan dust intrusions also known as “calima”, which consist of a mass of hot air or heat haze that can reach much more height than a sandstorm [19]. Their occurrence is especially remarkable from January to March and the most intense events take place in winter [20]. Although this phenomenon is very recurrent in the islands, only a few severe episodes are registered per year [21,22]. In February 2020, the archipelago was affected by a severe Saharan dust intrusion that broke the record in regard to intensity since instrumental data came to exist.

The objective of this research is to study the microbial communities found in dust particles and iberulites from the Canary Islands. To our knowledge, no studies on culturable microorganisms and mineral–bacteria interactions have been conducted in the Canary Islands. For that reason, dust samples have been collected in order to analyse their microbial diversity, mineralogical compositions and potential geomicrobial connections. This work lays the groundwork for subsequent studies that can shed light on microbial transport patterns and enhance our understanding of extremophilic life within the Earth’s atmosphere.

## 2. Materials and Methods

### 2.1. Sampling Site

This study was conducted in the municipality of Teror (Gran Canaria, 28°03′31.6″ N, 15°32′58.2″ W), located in the Canary Islands (Figure 1). The weather is characterized by prevailing trade winds blowing north to northeast and the influence of the “Canary Current”, which flows in a northeast–southwest direction. The latitude and the weather conditions contribute to a milder-than-normal climate for the islands [21].

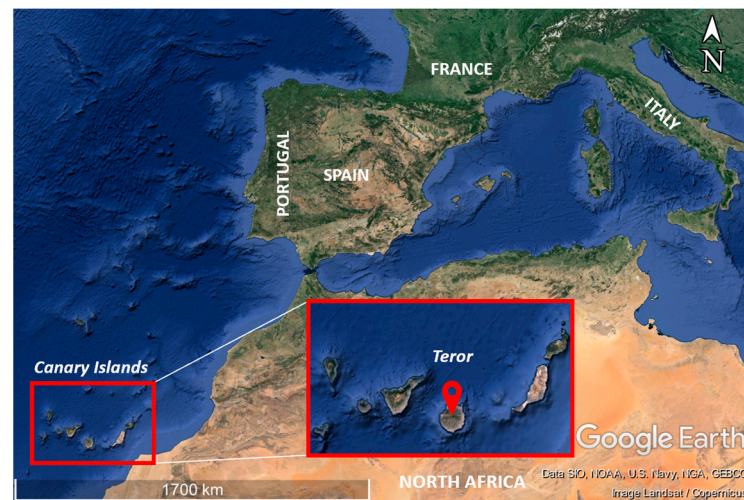


**Figure 1.** Description of the sampling area. Images retrieved from Google Earth.

## 2.2. Collection of Dust

Dust samples were collected during three different events of Saharan dust intrusions bound to calima episodes (Table 1). For that purpose, we used a glass collector (17.5 cm diameter) previously sterilised in an autoclave (at 121 °C for 20 min).

**Table 1.** Description of dust samples from African sources.

Sample	Sampling Date	Period of the Event	PM10 ( $\mu\text{g}/\text{m}^3$ )
M1	2 October 21	1–3 October 2021	47.0
M2	6 February 22	1–14 February 2022	65.4
M3	17 April 22	16–19 April 2022	54.3

## 2.3. Recognition and Selection of Iberulites

Sample M1 was initially screened under an Olympus B061 stereomicroscope to examine the content of iberulites. Then, iberulites were separated from the surrounding material and carefully hand-picked with a magnetized needle to avoid breakage.

## 2.4. Identification of Dust Sources and Characterization of the Events

Records of African dust intrusions over the Canary Islands were obtained [23,24] to determine the events registered at the sampling site. Dust surface concentration maps were acquired using the MONARCH model (<https://dust.aemet.es/products/daily-dust-products> (accessed on 7 May 2022)) [25,26] to ascertain the source and analyse the distribution of each event.

The Hybrid Single Particle Lagrangian Integrated Trajectory model (HYSPLIT) (<https://www.ready.noaa.gov/HYSPLIT.php> (accessed on 7 May 2022)) [27] was used to obtain 72 h backward trajectories, with the aim of determining the source region of the air masses bound to each dust intrusion. To that end, we used the vertical velocity model, and the altitude was set to 750, 1500 and 2500 m.a.g.l., respectively. The length of each backward trajectory was measured in Google Earth.

The mean PM10 concentration—registered during the sample collection period—bound to each dust event was estimated (Table 1) using data from the “Polideportivo Afonso-Arucas” station, located in the North of Gran Canaria (28°06′41″ N, 15°31′15″ W). The station cited previously belonged to the “Red de Vigilancia y Control de la Calidad del Aire de Canarias” [28].

### 2.5. Munsell Colour

Dust colour was determined using Munsell soil charts.

### 2.6. Granulometry

The particle size distribution of bulk dust dispersed in water was determined by laser diffraction on a Mastersizer 2000LF (CIC, Universidad de Granada). Granulometric results were interpreted using the Mastersizer 2000, v.5.61 software ([www.malvernpanalytical.com](http://www.malvernpanalytical.com) (accessed on 7 May 2022), Malvern, UK). Analyses were only performed on samples M1 and M2; the quantity required was not obtainable in sample M3.

### 2.7. Mineralogical Composition

Mineralogical composition was determined by XRD diffraction on a Bruker AXS D8 ADVANCE diffractometer equipped with a PILATUS3R 100K-A detector (Bruker, Germany). The measurement parameters were Cu K $\alpha$  radiation, 1.5406 wavelength ( $\lambda$ ) and an exploration range from 3° to 75° 2 $\theta$ . XRD diagrams were interpreted using the Xpovder software (Ver. 12) [29]. Percentages of each mineral phase were estimated from the intensity factors [30–32]. Analyses were only performed on samples M1 and M2; the quantity required was not obtainable in sample M3.

### 2.8. Surface Chemical Composition

Surface chemical composition was obtained by X-ray photoelectron spectroscopy (XPS) on a Kratos Axis Ultra-DLD spectrometer equipped with Al K $\alpha$  source (Kratos Analytical Ltd., Kyoto, Japan). For a wide scan, a pass energy of 160 eV was applied. The binding energies were calibrated with reference to C1s at 284.8 eV. Spectra were interpreted using CasaXPS v2.3.16 Pre-rel 1.4 software ([www.casaxps.com](http://www.casaxps.com) (accessed on 7 May 2022), Casa Software Ltd., Devon, UK). Analysis was only performed on sample M1.

### 2.9. Microscopy Analyses

Iberulites were visualized by confocal laser scanning microscopy (CLSM) on a Leica TCS-SP5 microscope (CIC, Universidad de Granada). Dust material and iberulites were studied through scanning electron microscopy, employing a GEMINI (FESEM) CARL ZEISS apparatus equipped with EDX-OXFORD10 (CIC, Universidad de Granada). To enhance the visualization of bacteria, samples were initially subjected to treatment with a solution of 2.5% glutaraldehyde in a 0.1 M cacodylate buffer, followed by 1% osmium tetroxide. Subsequently, they were subjected to dehydration with alcohol, dried through the critical point method and eventually coated with carbon, as previously described [33]. Measurements of maximum diameter were made using the images, with IC Measure v.2.0.0.286 software (The Imaging Source, Bremen, Germany).

### 2.10. Isolation of Culturable Microorganisms

For the study of culturable microorganisms, dust particles were deposited on plates with 10% Trypticase Soy Agar (TSA) medium and incubated at room temperature. The serial dilution method was used for the isolation of microorganisms, and a preliminary identification was carried out by Gram staining.

### 2.11. Identification of Isolated Culturable Microorganisms

Isolated culturable microorganisms were identified by partial sequencing of the 16S rRNA gene. The “DNA Xtrem” kit was employed to extract DNA. Subsequently, universal bacterial primers, 16F27 and 16R1492, were utilized for PCR amplification. The resulting PCR products were then purified using the X-DNA purification kit (QIAquick PCR Purification Kit 250).

Direct sequence determination of PCR-amplified DNA was carried out with the ABI PRISM dye-terminator, cycle-sequencing, ready-reaction kit (Perking-Elmer) and an ABI PRISM 377 sequencer (Perking-Elmer), according to the manufacturer’s instructions. The



obtained sequences were visualized using Chromas 2.6.6 software (Chromas) and were compared to reference 16S rRNA gene sequences available in the GenBank, EMBL and DDBJ databases through the BLAST search [34] and the EzBioCloud server [35].

### 3. Results

#### 3.1. Identification of Dust Sources Linked to Calima Episodes

The three dust events studied (samples M1–M3) were bound to African dust intrusions (Table 1 and Figure 2). Sample M1 travelled the longest distance (around 1824 km), followed by samples M3 and M2 (Table 2). PM10 concentration during each event was variable, ranging from 47.0 to 65.4  $\mu\text{g}/\text{m}^3$  (Table 1).

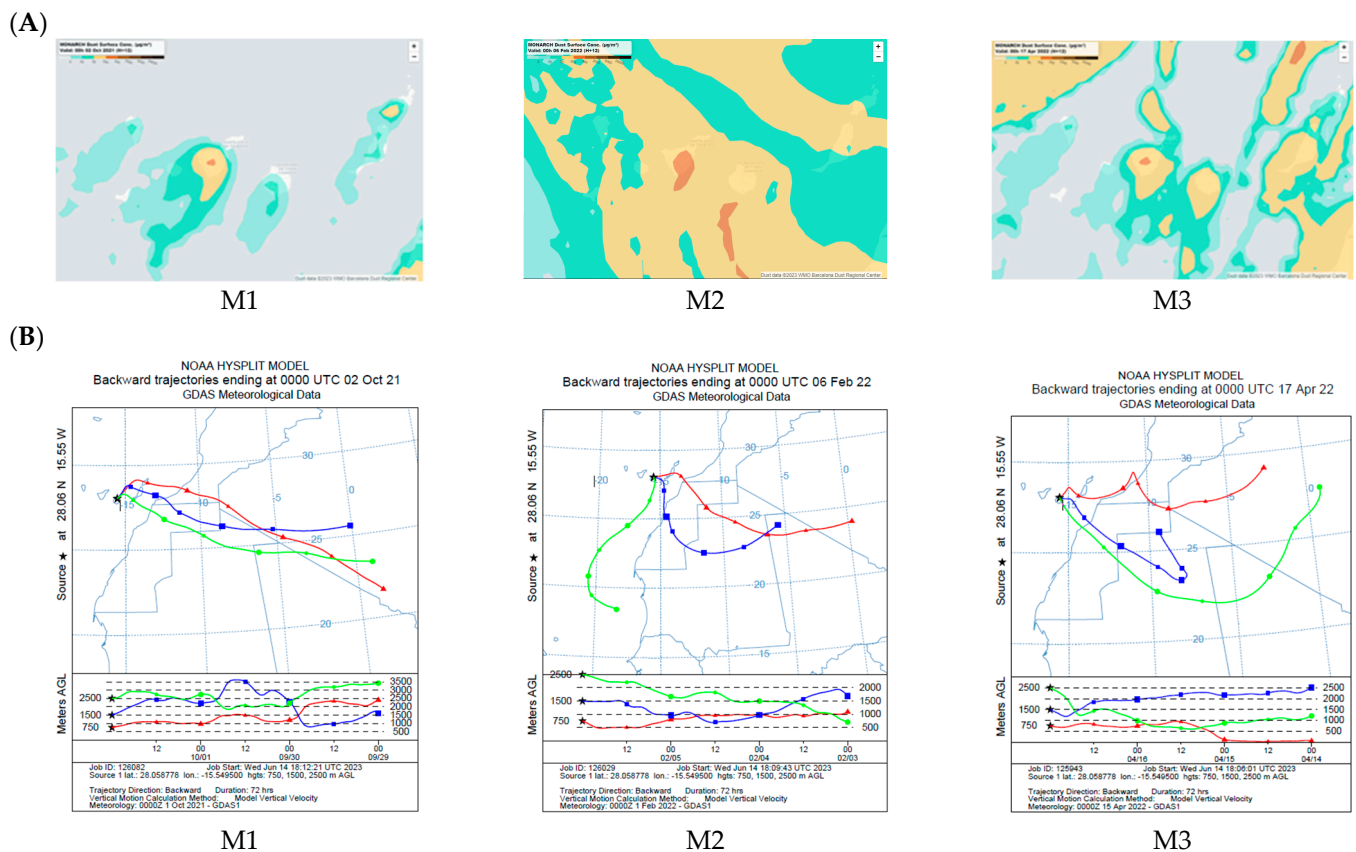


**Figure 2.** Identification of the dust source of the events associated with each sample: M1, M2 and M3. (A) Dust concentration maps (MONARCH model, dust surface concentration  $\mu\text{g}/\text{m}^3$ ). (B) Backward trajectories (at different altitudes): 750 m (red), 1500 m (blue) and 2500 m (green).

**Table 2.** Lengths of the backward trajectories (km). Data obtained from Google Earth.

Sample	Height			
	750 m	1500 m	2500 m	Mean
M1	1997.14	1670.67	1803.3	1823.70
M2	1813.57	1498.48	1417.04	1576.36
M3	1591.13	1301.58	2238.93	1710.55

#### 3.2. Colour of Dust Samples

Shades (hue) were variable according to Munsell notation (Table 3). Sample M1 belonged to 7.5YR; samples M2 and M3 corresponded to 10YR. The percentage of red pigment (5R–100%, 5YR–50% and 5Y–0%) ranged from 25% to 37.5%, with the major proportion detected in sample M1. Lightness (value) and saturation (chroma) showed a

descending trend, since both attributes were higher in sample M1 (5/3.5) and decreased in samples M2 (4/2.5) and M3 (3/2).

**Table 3.** Colour of dust samples (M1–M3).

Sample	Notation	Name	Hue	Hue% red	Value	Chroma
M1	7.5YR 5/3.5	Brown	7.5YR	37.5	5	3.5
M2	10YR 4/2.5	Dark greyish brown	10YR	25.0	4	2.5
M3	10YR 3/2	Very dark greyish brown	10YR	25.0	3	2
			Mean	29.2	4.0	2.7

### 3.3. Particle Size Distribution of Dust Samples

Mean granulometric results showed that dust samples were mainly composed of 59% silt (2–50  $\mu\text{m}$ ), 34% sand (50–2000  $\mu\text{m}$ ) and 7% clay (<2  $\mu\text{m}$ ) (Table 4). The mean PM<sub>2.5</sub> and PM<sub>10</sub> contents were around 7% and 24%, respectively.

**Table 4.** Granulometry (%). Samples M1 and M2.

Sample	Clay (<2 $\mu\text{m}$ )	Silt (2–50 $\mu\text{m}$ )	Sand (50–2000 $\mu\text{m}$ )
M1	10.3	70.3	19.4
M2	4.6	47.9	47.6
Mean ( $n = 2$ )	7.4	59.1	33.5

Sample M1 (Figure 3), proximate to a complex Gauss bell, has a bimodal distribution, with a main peak in the silt fraction (15–20  $\mu\text{m}$ ) and a secondary peak in the sand fraction (350–500  $\mu\text{m}$ ). Sample M2 (Figure 3) shows a unimodal distribution, with a main peak in the sand fraction (60–90  $\mu\text{m}$ ); it also hints at a secondary peak in the sand fraction (300–600  $\mu\text{m}$ ).

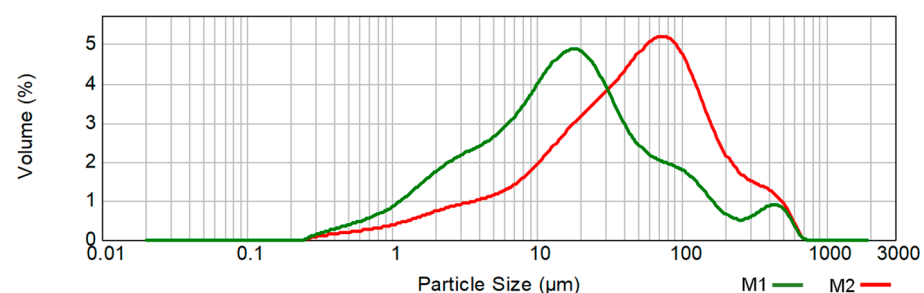


**Figure 3.** Particle size distribution. Samples: M1 (green) and M2 (red).

Statistical parameters related to the particle size distribution (Table 5) revealed that the mean diameter of dust particles was around 65  $\mu\text{m}$ . Both samples show a leptokurtic distribution (kurtosis > 3; mean = 11.083) and are positively skewed (skewness > 0; mean = 3.073).

**Table 5.** Statistical parameters related to particle size distribution.

Statistics	Mean ( $\mu\text{m}$ )	Standard Deviation ( $\mu\text{m}$ )	Kurtosis	Skewness
M1	45.593	87.938	15.500	3.723
M2	83.256	103.569	6.666	2.422
Mean ( $n = 2$ )	64.425	95.754	11.083	3.073

The maximum diameter of iberulites ( $n = 23$ ) was measured (Figures 6 and 7). The mean size was approximately 110  $\mu\text{m}$ , ranging from 50.9 to 193.5  $\mu\text{m}$ .

### 3.4. Mineralogical Composition

Dust samples (M1, M2) were composed of the following mineral phases (Table 6 and Figure 4): phyllosilicates (clay minerals and chlorite), tectosilicates (quartz, k-feldspar and plagioclase), carbonates (calcite and dolomite), iron oxides (haematites) and gypsum. Phyllosilicates (39–59%) and tectosilicates (32–41%) were the main constituents. Carbonates (5–15%), iron oxides (4–5%) and gypsum (<1%) were present in minor proportions. Other mineral phases belonging to the group of clay minerals were qualitatively identified (Figure 4): smectite, palygorskite, illite, kaolinite and mixed-layer clay minerals.

**Table 6.** Mineralogical composition (%).

Sample	Gy	CM *	Chl	Qz	Fd-K	Pl	Ca	Do	OxFe
M1	<0.1	58	1	22	6	4	2	3	4
M2	<1	37	2	22	13	6	11	4	5
Mean ( $n = 2$ )	<0.1	48	2	22	10	5	7	4	5

Legend: gypsum (Gy), clay minerals (CM), chlorite (Ch), quartz (Qz), K-feldspar (Fd-K), plagioclase (Pl), calcite (Ca), dolomite (Do), iron oxides (OxFe). \* CM: smectite (Sm), palygorskite (Pal), illite (Ill), paragonite (Pa), kaolinite (Ka) and mixed-layer clay (MLC).

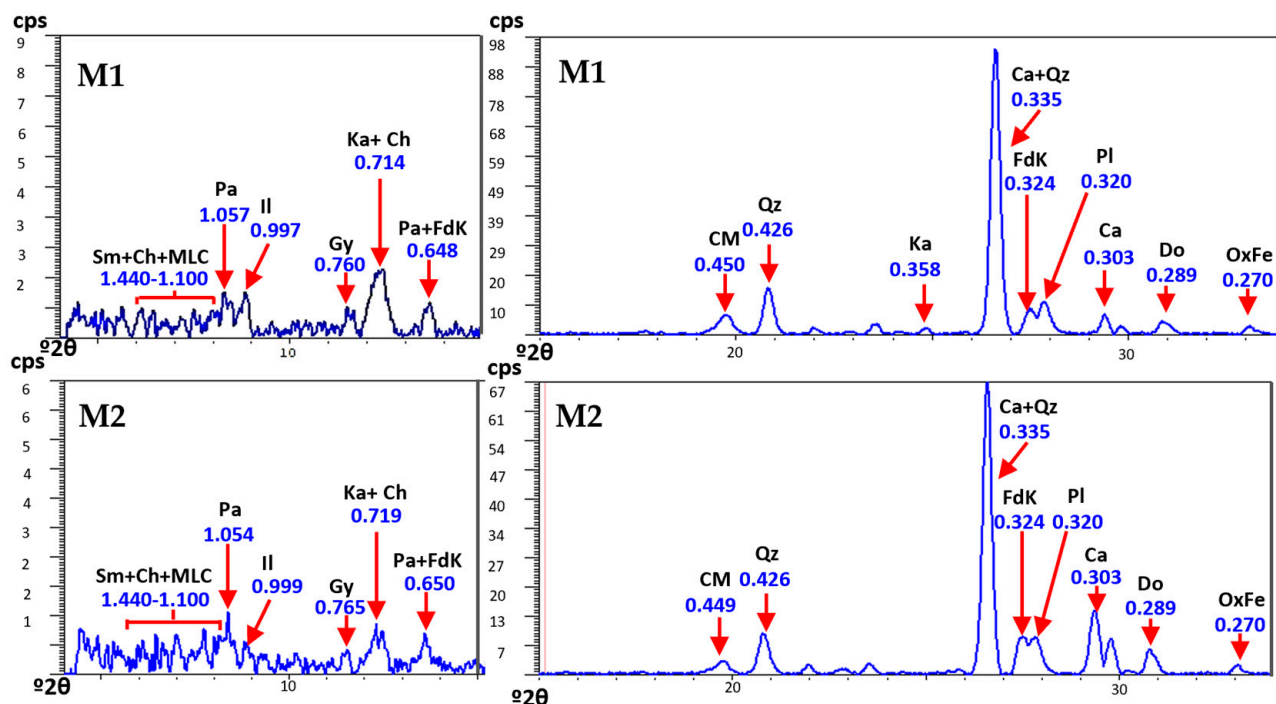


**Figure 4.** XRD diagrams. Samples M1 and M2.

### 3.5. Surface Chemical Composition

The XPS spectrum of sample M1 (Figure 5 and Table 7) revealed that the main constituents were O (47.97%), Si (16.03%) and C (15.64%); Al (7.45%) was detected in an intermediate proportion. Some elements such as Fe (4.40%), Ca (2.33%), Na (1.56%), Mg (1.37%) and K (1.01%) were found in minor proportions; N, Cl, S, Zn and P were present in trace amounts (<1%).

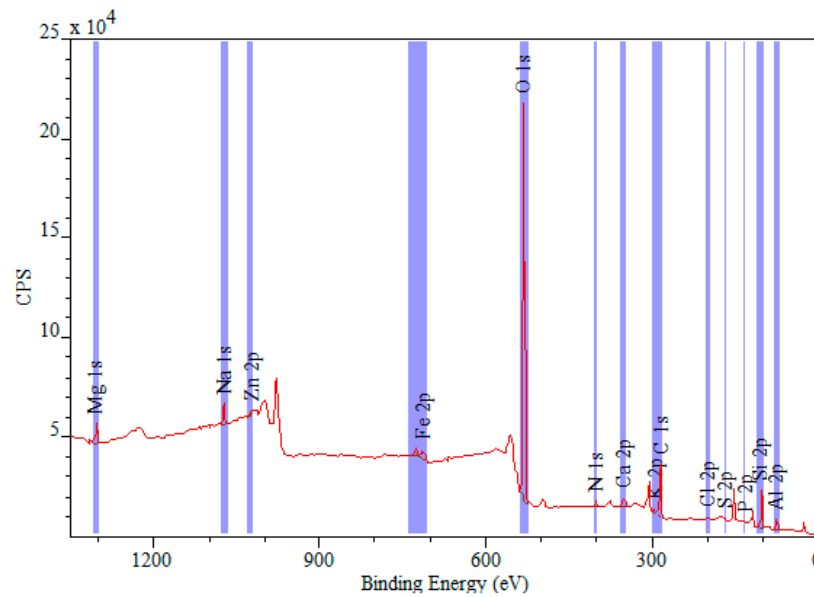


Figure 5. XPS survey spectrum. Sample M1.

Table 7. Surface chemical composition (% mass concentration). Sample M1.

C	O	N	Ca	Si	Na	Mg	Al	Cl	S	P	K	Fe	Zn
15.64	47.97	0.96	2.33	16.03	1.56	1.37	7.45	0.57	0.27	0.16	1.01	4.4	0.27

### 3.6. Microscopy Analyses

Iberulites were visualised by CLSM for the first time, with this being a novel technique unemployeed in the literature until now. Figure 6 shows a group of iberulites with an average diameter of approximately 115  $\mu\text{m}$ , with their characteristic vortex being visible in some of them. Single red fluorescent particles distributed over iberulites' surfaces indicate the existence of organic material.

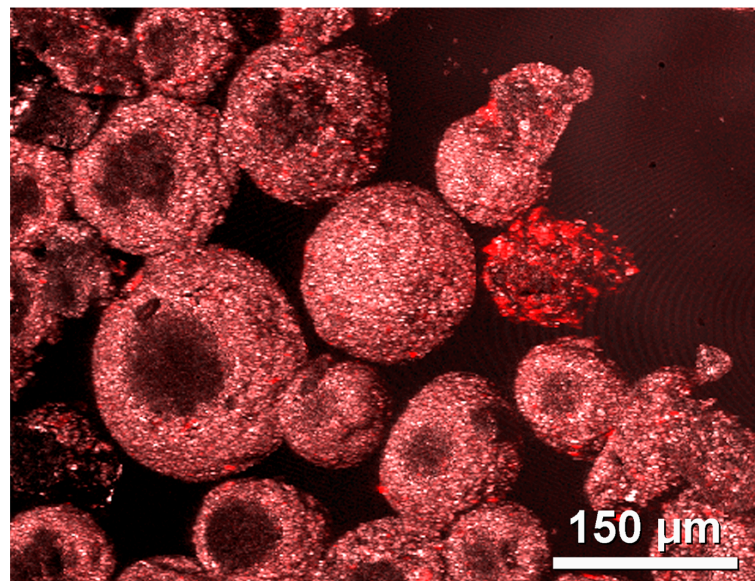
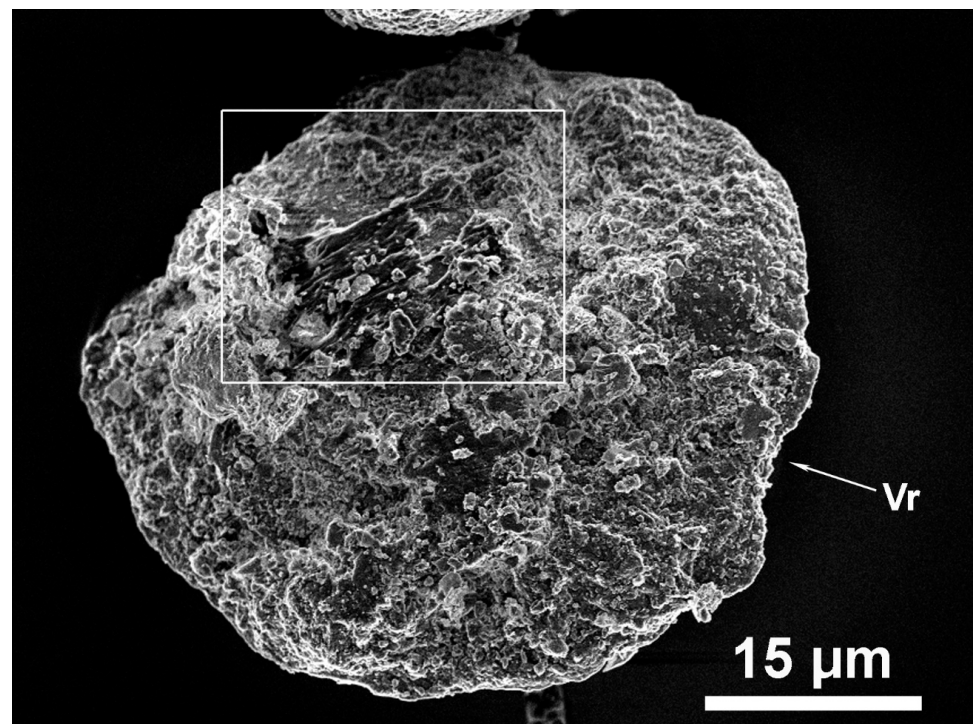


Figure 6. Confocal laser micrographs of non-stained iberulites (87.1–193.5  $\mu\text{m}$ ). The organic material shows slightly high red autofluorescence. The vortex is visible in most of them, although it appears expanded and distorted because of the loss of coherence, due to the preparation for observation.



A quasi-spherical iberulite of around 50  $\mu\text{m}$  diameter was observed by SEM-EDX (Figure 7). We identified some typical features such as the vortex (Vr) and the external rind, the latter being partially covered by a biofilm (BF) and some filaments (Figure 8).



**Figure 7.** Iberulite of 50.94  $\mu\text{m}$  diameter and quasispherical morphology, observed in a sideways position. The orifice of vortex (Vr) is not visible.

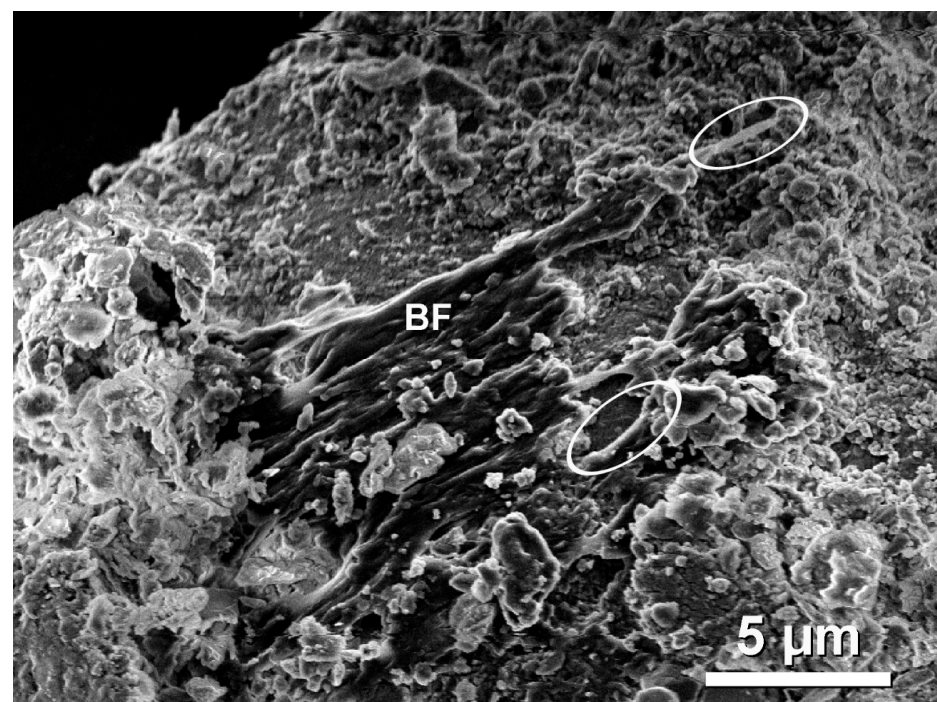


**Figure 8.** Detail of the upper image, of the field marked with a rectangle (Figure 7). The iberulite surface is partially covered by a dark, mucilaginous biofilm (BF) in formation and some filaments (marked with ellipses).

The mineralogical composition of dust (Table 6) was also corroborated by SEM-EDX. A quartz grain of around 20  $\mu\text{m}$  with evidence of aeolian modelling is displayed in Figure 9.

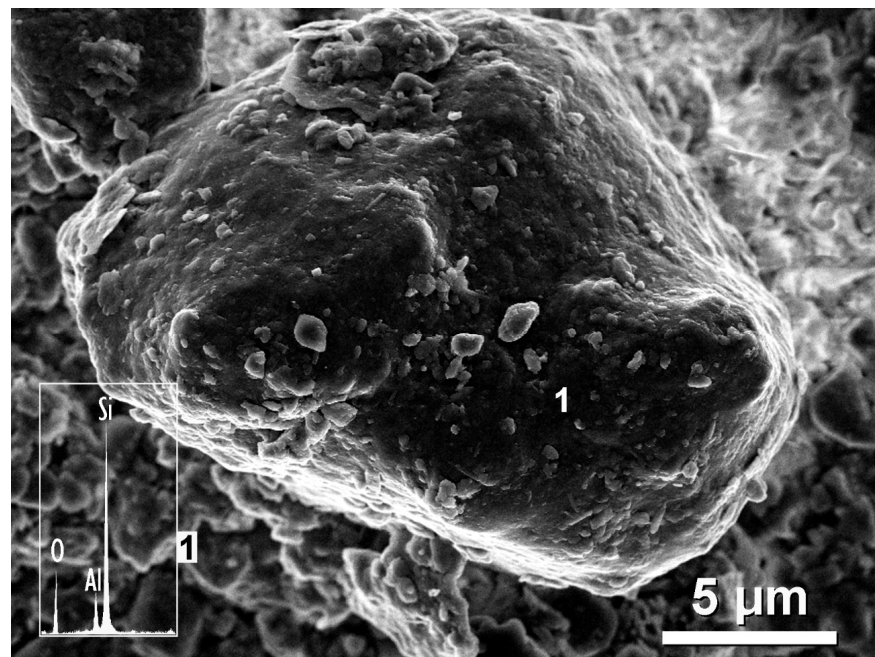


**Figure 9.** Mineral grain with a diameter of 21.71  $\mu\text{m}$ . Chemical composition: 1. EDX, Si, O, Al (quartz). The roundness observed is due to wind erosion (aeolian modelling). The surface is covered by quite nano-sized particles, some of them with ellipsoidal morphologies which resemble possible bacteria.

The interaction between bacteria and mineral particles was also illustrated. Figures 10 and 11 depict a bacterial cell (BC) over the surface of a dolomite particle, and a group of rod-shaped bacteria in a colony (MC) as part of a mineral particle aggregate. Likewise, several bacterial cells associated with kaolinite particles (Kln) were also found (Figure 12).

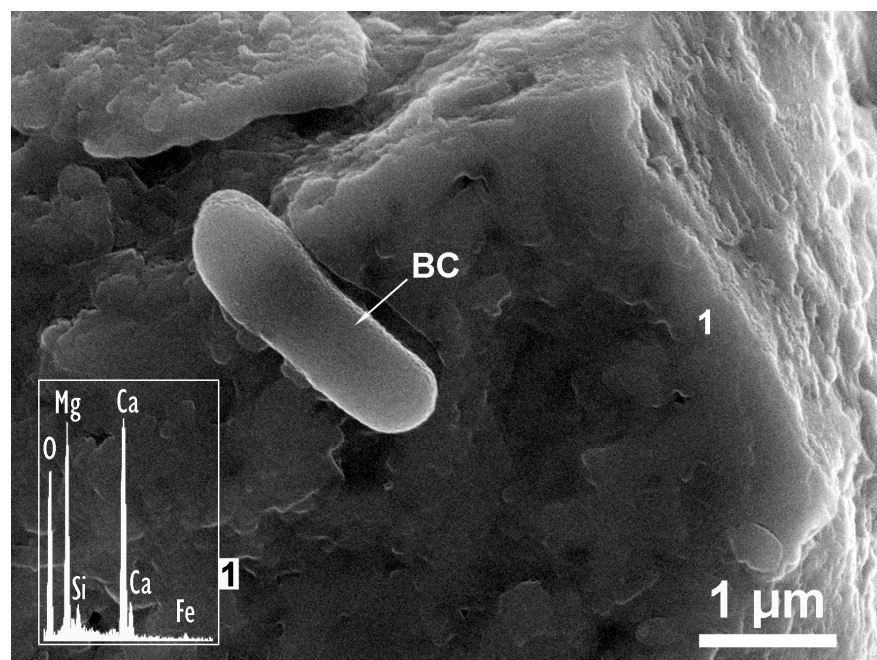


**Figure 10.** Bacterial cell (BC) of 2.3  $\mu\text{m}$  length over a mineral grain with a complex microtopography. Chemical composition: 1. EDX, Ca, Mg, O, Si, Fe (dolomite).



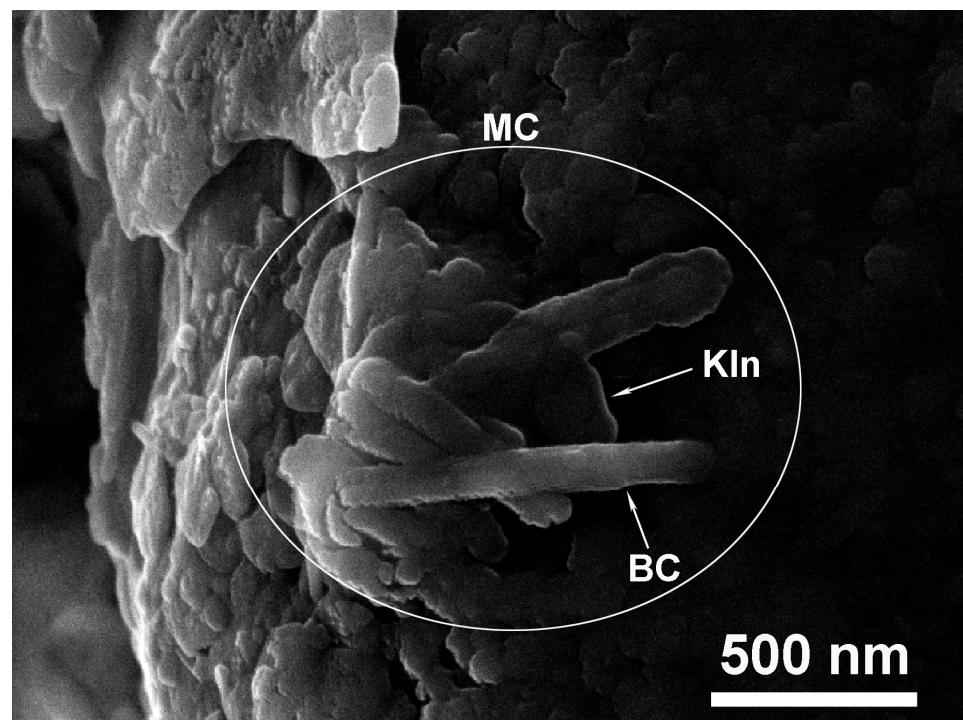


**Figure 11.** Microbial colony (MC) as part of a mineral particle aggregate. Some bacterial cells (BC) can be observed over a pseudo-hexagonal kaolinite crystal (Kln).

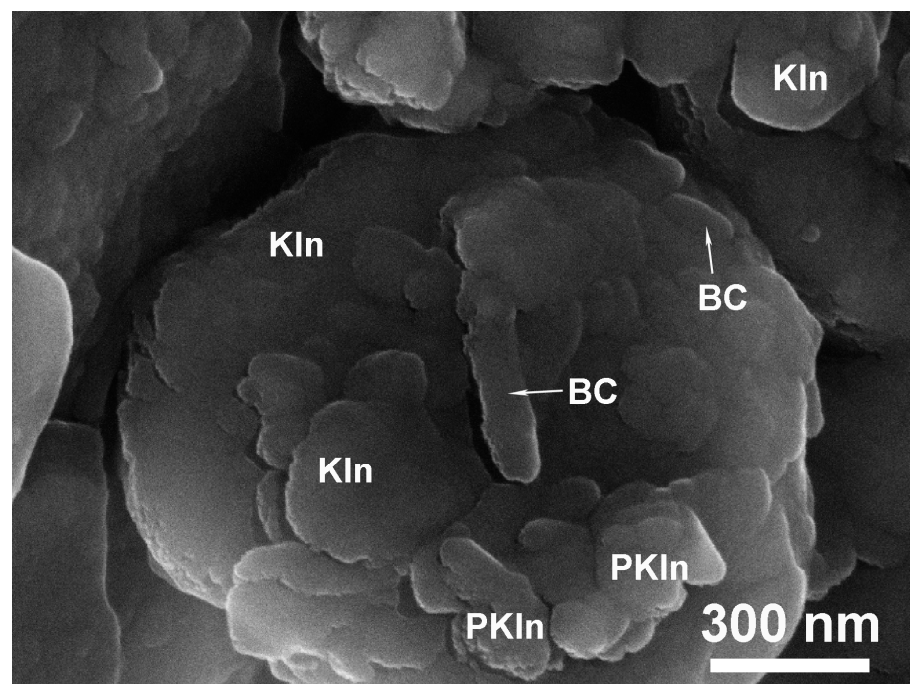


**Figure 12.** Bacterial cells (BC) immersed in a process of induced biomineralization of pseudo-hexagonal kaolinite crystals (Kln) of lamellar habit at different stages of mineral reorganization. Protokaolinite (PKln) gels can be seen, as well as the outline of a large pseudo-hexagonal kaolinite crystal.

### 3.7. Identification of Microorganisms Isolated from Dust Samples

A total of twenty-three culturable microorganisms were isolated after preliminary characterization. Most of them were bacilli, with 44% being Gram-positive and 30% Gram-negative. Additionally, 13% Gram-positive cocci and 13% Gram-negative cocci were isolated. Figure 13 shows the percentage of culturable microorganisms isolated in

each sample according to their preliminary characterisation by Gram staining. Bacterial abundance was estimated from the number of isolated culturable microorganisms per sample (ncm).

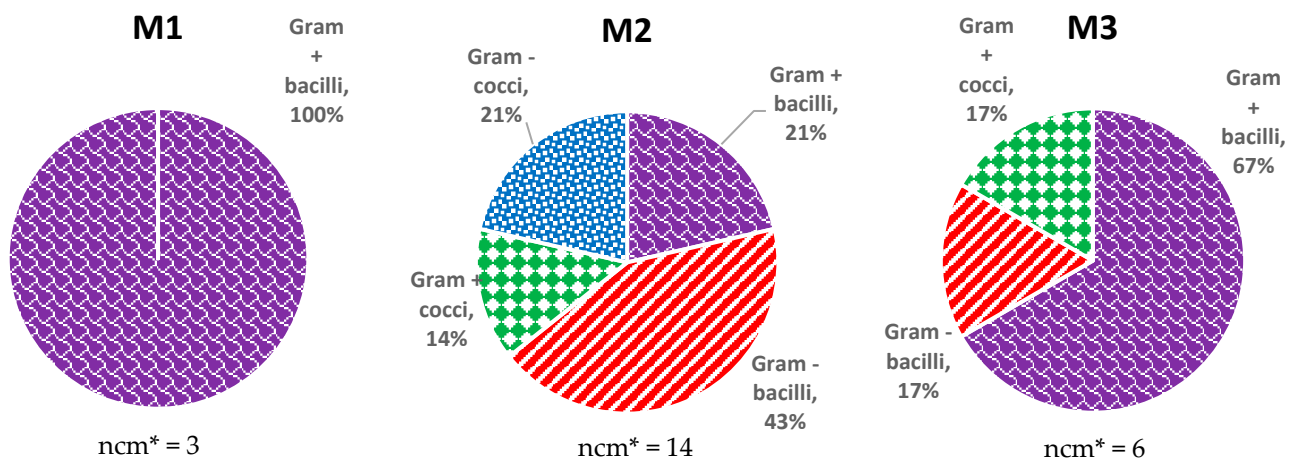


**Figure 13.** Isolated culturable microorganisms. Classification according to Gram staining (\* Number of culturable microorganisms (ncm) isolated per sample).

Nineteen of the isolated microorganisms were identified by means of 16S rRNA sequencing, corresponding to *Pseudomonadota*, *Bacillota* and *Actinomycetota* phyla (Table 8).

**Table 8.** List of microorganisms identified. The taxa, strains and percentage identities of the 16S rRNA gene sequences are indicated.

N°	Sample	Taxon	Strain	Identity (%)
1	M1	<i>Niallia circulans</i>	ATCC 4513(T)	98.81
2	M2	<i>Micrococcus luteus</i>	NCTC 2665	99.84
3	M2	<i>Bacillus toyonensis</i>	BCT-7112	99.29
4	M2	<i>Acinetobacter lwoffii</i>	NCTC 5866	99.83
5	M2	<i>Enterobacter cancerogenus</i>	ATCC 33241(T)	99.21
6	M2	<i>Paracoccus aereus</i>	011410	98.86
7	M2	<i>Pseudeschherichia vulneris</i>	NBRC 102420	99.33
8	M2	<i>Exiguobacterium artemiae</i>	9AN	99.83
9	M2	<i>Glutamicibacter soli</i>	SYB2	99.85
10	M2	<i>Pseudomonas alloputida</i>	Kh7(T)	99.26
11	M2	<i>Bacillus safensis</i> subsp. <i>safensis</i>	FO-36b	99.93
12	M2	<i>Pseudomonas hunanensis</i>	LV(T)	99.41
13	M2	<i>Sanguibacter inulinus</i>	ST50	100.0
14	M3	<i>Peribacillus frigoritolerans</i>	DSM 8801	98.59
15	M3	<i>Bacillus safensis</i> subsp. <i>safensis</i>	FO-36b	99.08
16	M3	<i>Pseudomonas juntendi</i>	BML3(T)	99.70
17	M3	<i>Paenarthrobacter nitroguajacolicus</i>	G2-1	99.68
18	M3	<i>Sanguibacter keddieii</i>	DSM 10542	99.66
19	M3	<i>Pantoea endophytica</i>	596(T)	98.69



## 4. Discussion

### 4.1. Identification of the Dust Sources and Description of the Events

Dust samples (M1–M3) had an African provenance, but some differences were found (Table 1 and Figure 2). The backward trajectories of all samples had a Saharan component, with sample M3 being purely from the Saharan desert. The dust source provenance of samples M1 and M2 was influenced by air masses from the Sahel region and the Atlantic Ocean, respectively. The distance travelled by each dust plume was also different (Table 2), with an influence on granulometry, mineralogy and bacterial diversity, as we will discuss later.

PM10 data (Table 1) revealed that the most intense event corresponded to sample M2, followed by sample M3 and sample M1. According to Rodríguez et al. (2015) [36] PM10 concentration tends to increase from tens to hundreds  $\mu\text{g}/\text{m}^3$  during these events in the archipelago, being our data consistent with these values.

### 4.2. Colour of Dust Samples

Dust samples showed different shades of brown (M1), dark greyish brown (M2) and very dark greyish brown (M3) (Table 3). Sample M1 was the most chromatic and contained the major proportion of red pigment. As previously stated, this sample travelled the longest distance and, therefore, it might imply a major dust redness due to a possible process of atmospherogenesis (defined later in Section 4.6).

### 4.3. Granulometry

Dust samples were mainly composed of silt particles, with minor proportions of sand and clay fractions (Tables 4 and 5 and Figure 3). Sample M1 had more silt (70%) than sand (20%), whereas sample M2 had a similar proportion of silt and sand (~48%). The mean diameter of the particles as well as the kurtosis value were also higher in sample M2 (83.3  $\mu\text{m}$ ), corroborating a major content of sand.

Granulometry was also endorsed by the length of backward trajectories (Table 2). The minor distance travelled by the dust plume would justify a coarser granulometry, and vice versa. Under this assumption, this statement would be proved in both cases (samples M1 and M2) (Figure 2).

The particle-size curves showed a unimodal (M2) and a bimodal distribution (M1); both distributions were previously described in other dust studies from the Canary Islands [19,37,38]. The differences could be attributed to the dust provenance from one source (Sahara) or several sources (Sahara and Sahel) [39].

Sample M1 contained a major proportion of PM2.5 and PM10 particles, which would also be consistent with a finer granulometry. Nevertheless, these data showed no correlation regarding the PM10 concentration level registered during the dust event.

The iberulites' sizes were mainly distributed between 50–150  $\mu\text{m}$  (39%) and 100–150  $\mu\text{m}$  (52%); only 9% of them were between 150–200  $\mu\text{m}$ . The mean diameter and the size range were in agreement with the values obtained by Díaz-Hernández & Párraga (2008) [17], but differed from other studies [18].

### 4.4. Mineralogical Composition

The mineralogical composition of dust was largely dominated by phyllosilicates and tectosilicates, with minor proportions of carbonates and iron oxides (Table 6, Figure 4). Sample M1 had a major proportion of clay minerals (59%), previously corroborated with a finer granulometry (Table 4), and the longest distance travelled (Table 2). In contrast, sample M2 was richer in K-feldspar (13%) and calcite (11%). Both samples contained the same proportion of quartz, and the rest of the mineral phases were almost constant.

Smectite, palygorskite, illite, kaolinite and mixed-layer clay minerals were identified within the group of clay minerals. Paragonite was not detected in our samples, in contrast to other studies of aeolian dust in the Iberian Peninsula; this mineral is absent in African soils but is typically found in Betic materials from southern Spain [18]. The presence of kaolinite was corroborated by SEM-EDX (Figures 11 and 12). Other mineral phases such as

palygorskite and smectite had previously been detected in Saharan dust [40], corroborating the African provenance.

The proportion of quartz considerably differed from other studies in the Canary Islands, which in turn reported a minor percentage of clay minerals [19,37]. Quartz has been described in dust of Saharan origin [41].

Carbonates and feldspars were found in intermediate proportions. Mineral dust containing a high abundance of carbonates (>10%, calcite > dolomite) is likely to have a North African provenance [42]. According to these authors, plagioclase and K-feldspars are also commonly found in minor proportions in African dust.

Haematites and gypsum were detected in minor proportions. Haematites are present in low proportions in topsoil of the Sahara Desert and the Sahel region [43]; this mineral species, along with goethite, would be responsible for the yellowish–reddish colour of desert soils [44]. The iron phases might also be involved in atmospheric processes, as will be discussed in Section 4.5. Gypsum has previously been described in soils from the Sahara and Sahel region [45]. This mineral could also be a product of atmospheric neof ormation due to the attack of atmospheric  $H_2SO_4$  on some primary minerals, such as smectites and calcite (both detected in our samples) (Table 6 and Figure 4) [17].

#### 4.5. Surface Chemical Composition

Due to the heterogeneity of the mineral surfaces in atmospheric dust, the XPS technique allows a close approximation to study their atomic composition. Si and Al were detected in abundant to intermediate proportions ( $Si \gg Al$ ) (Table 7 and Figure 5). The binding energy values were compatible with  $SiO_2$  and aluminosilicates, being consistent with the proportions of both quartz and clay minerals (Table 6) [46]. Additionally, although K and Mg were found in trace amounts, both showed a binding energy in agreement with muscovite and montmorillonite [47]. The low proportions of these elements would indicate that they belong to the internal crystalline lattice.

C was also dominant in the dust surface, in contrast to the percentage of carbonates found by XRD (Inorganic C). The proportion of inorganic C (0.63%), estimated from calcite ( $CaCO_3$ ) and dolomite ( $MgCaCO_3$ ) quantities, was extremely low compared to total C (XPS) (15.67%). The presence of organic matter in the dust surface would justify the prevalence of organic C (96%) over inorganic C from carbonates (4%). Organic matter has a great affinity for adsorption on mineral surfaces such as aluminosilicates, quartz and iron oxides. In addition, the Si/Al ratio obtained by XPS would support this affinity for clay minerals [48].

The binding energy of Fe corresponded with iron oxides ( $Fe_2O_3$ ) [49] and, therefore, this would be corroborated by the presence of haematites. However, differences between total Fe (XPS) and haematites (XRD) were observed. The proportion of Fe (XRD) (2.8%) from haematites ( $Fe_2O_3$ ) was lower than the total Fe (XPS) (4.4%), which also included free iron. In this case, free iron (63.64%) would predominate over haematites (36.36%) in the dust surface. Aggregates of iron oxides are often in association with aluminosilicate platelets, indicating the existence of iron films over mineral particles, owing to the affinity of their reactive surfaces [50].

The presence of Ca and Na revealed important information. The binding energy of Ca might correspond to calcium phosphate and calcium carbonate [51], with the latter being consistent with calcite (Table 6). Similarly, Na and Cl had a binding energy in agreement with sodium chloride (NaCl) [46,52]. Halite (NaCl) was not detected by XRD, but this is not surprising as it is not commonly found in North Africa. Thus, the origin of this compound might be due to the enrichment of mineral dust with sea salt particles [42].

The presence of N and several minor elements is also noteworthy. N and P had binding energy values compatible with the presence of ammonium and phosphate, respectively [53]. The binding energy of S was in agreement with sulphates, namely gypsum, as previously detected by XRD (Table 6) [46]. The interaction of the mineral particles with anthropogenic compounds ( $NO_x$  and  $SO_x$ ) might increase the amount of secondary aerosols during

Saharan dust intrusions in the Canary Islands [54]. This process could also result in the neoformation of sulphates such as gypsum and alunite ( $\text{KAl}_3(\text{SO}_4)_2(\text{OH})_6$ ) [17].

Trace amounts of Zn were also detected in dust, showing a binding energy that might correspond to ZnO [55]. Although Zn has previously been detected during Saharan dust intrusions, it is mainly associated with road traffic and non-exhaust vehicle emissions [56].

#### 4.6. Microscopy Analysis of Iberulites and Dust Samples

CLSM revealed the presence of organic matter in the iberulites' surfaces (Figure 6). This finding would be supported by surface chemical composition analysis (XPS), indicating a high proportion of organic C in the dust particles' surfaces (Table 7).

New evidence of biological activity in iberulites was recognised through SEM (Figure 7). The iberulite rind was partially covered by some filaments (Figure 8). On the biofilm, some polymicrobial aggregates co-associated with entrapped mineral particles were observed. Biological spore-like forms in the external rind were previously visualised in iberulites, suggesting that active biologic agents might be transported attached to cavities, crevasses, cracks and any other surface irregularities in the external rind [16]. Thus, iberulites would provide protection against UV and a nutritive medium for microorganisms, acting as a potential source of microorganisms beneficial for plant growth.

Mineralogical composition was also illustrated by the SEM images. Figure 9 illustrates a quartz grain, a major constituent in dust samples. The general roundness would evidence the aeolian transport. Ellipsoidal nano-sized particles over the surface might be bacterial cells or spores, providing new evidence of the biological activity in atmospheric dust. Favet et al. (2013) [57] observed similar morphologies in sand from Saharan soils.

The mineral–bacteria association was clearly suggested by SEM. Figures 10–12 show different examples of microorganisms attached on mineral surfaces or as part of mineral aggregates. During atmospherogenesis processes, mineral particles can also form unions or even cover bacterial cells, with these being either isolated or in colonies. Figure 10 depicts a bacterial cell over a mineral grain of dolomite. Figure 11 illustrates a bunch of bacteria, a small colony, merged in an aggregate of mineral particles, in which the presence of a kaolinite particle is hinted. In Figure 12, some bacteria appear to be partially covered by tiny platelets, which might be kaolinite particles due to their crystal habit (with some clear hexagonal edges). These particles seem to be neoforming and regrowing amid the space they share with microorganisms.

The relationship between bacteria and mineral particles in the atmospheric dust studied here is demonstrated with SEM. This relationship can be formulated using at least four different approaches:

- (1) Bacteria might use the mineral surfaces to achieve major stability and stay in the air for a longer time period, creating polymicrobial interactions in close spatial association during the transport. Thus, both dust particles and iberulites contribute primarily to the transport and dispersion of microorganisms in the atmosphere in a continuous and essential process [58].
- (2) Bacteria seem to grow and even form colonies over particles, provided humidity is high enough, in microsites within mineral particles (Figure 11), aggregating around them. Dust suspended in the air would account for a unique culture medium, as a kind of soil solution, though it has never been described as such.
- (3) The third piece of evidence, and the most noteworthy, is the relationship between microorganisms and larger airborne particles—the iberulites—which resembles a “symbiosis”, in this case, between biotic and abiotic material. Both subjects receive a mutual benefit and share a particular bond, creating polymicrobial aggregates. On the one hand, microbial cells find shelter and protection against UV radiation and extreme temperatures. Microsites within mineral particles might retain some water and scarce nutrients, being subsequently suitable for bacterial growth. On the other hand, mineral particles improve their consistence owing to the bacterial

exopolysaccharides, which may act as cement, co-adjuvant or, in other words, as an aggregating substance for agglomeration; a biofilm (Figure 8).

- (4) The last piece of evidence would account for bacterial participation in the processes of atmospherogenesis in mineral dust. We understand “mineral atmospherogenesis” as the genesis of minerals within the atmosphere. When the action or presence of living beings is needed for mineral genesis, it is known as “mineral bioatmospherogenesis”. The case shown in Figure 12 (also observed in Figure 11) is remarkable. It suggests atmospheric biotic participation in the neoformation process of kaolinite, a clay mineral commonly found in supergene environments. This fact has been observed for the first time here and will require further research, but if confirmed, it would be classified as “mineral bioatmospherogenesis”.

The role of bacteria, as possible inductors of kaolinite neoformation, might imply the release of organic compounds (some of them acid). Then, bacteria would facilitate the hydrolysis of some primary aluminosilicate mineral particles and the subsequent neoformation of Al and Si gels (protokaolinite), which turn into authentic kaolinite sheets through growth. Likewise, these sheets would merge and encapsulate bacterial cells, as illustrated in the images.

Until now, mineral synthesis and kaolinite neoformation processes had only been described in some modern natural environments and laboratory experiments [59–62]. These processes had never been described in the atmosphere and let alone, mediated by atmospheric microbiota via a process known as bacteria-induced mineral [63–65] precipitation [66]. Other organic compounds present in dust—not necessarily microbial—might collaborate in the atmospherogenesis of kaolinite, being that their presence was previously proved in the elemental surface composition (XPS) (Table 7).

#### 4.7. Description of Culturable Microbial Communities

Microorganisms are ubiquitous in the environment, and the atmosphere is no exception. However, airborne bacterial communities remain relatively unexplored. Enhancing our understanding of these communities and the mineral composition of dust particles is crucial for comprehending the impact on biodiversity and health.

In total, 23 culturable microorganisms were isolated, being mostly present in samples M2 (ncm = 14) and M3 (ncm = 6) (Figure 13). In contrast, sample M1 showed the lowest number (ncm = 3). As previously stated, sample M1 not only had a finer granulometry, but also the longest backward trajectory compared to sample M2 (Tables 2 and 4 and Figure 2). The major distance travelled might imply a major dust elevation from the soil on the ground, causing a bacterial deprivation. Furthermore, the backward trajectory’s length, corroborated by the wind speed, would justify the residence time in the atmosphere, compatible with the time needed for bacterial growth (Table 2).

Prior studies revealed that the bacterial abundance depended on dust granulometry [63–65]. The major abundance corresponded to sample M2, with its coarser granulometry and minor percentage of clay minerals (Tables 4 and 6, Figures 3 and 4). Stern et al. (2021) [65] observed a higher bacterial abundance in coarse particles (particles > 10 µm), likely being derived from local sources. In our case, the highest bacterial abundance bound to the coarser granulometry might be attributed to the atmospheric dust genesis, considering the minor distance from soil. Thus, bacteria would travel attached to mineral particles or inside polymineral aggregates with strategic microsites suitable for bacterial growth. The visualisation of bacteria over the surface of mineral particles, as well as the geomicrobial interactions observed by SEM-EDX, would support these statements (Figures 7–12).

Particle size had also an influence on the airborne bacterial communities. Some studies found that spore-forming microorganisms were more abundant in large particles, whereas viable microorganisms were mostly present in particles of reduced size [63,64]. Additionally, Stern et al. (2021) [65] reported a major abundance of pathogens in fine particles (particles < 2.5 µm), which can be suspended in air for a longer period of time.



Therefore, fine particles pose a threat to human health due to their biological content and respirable size.

In total, 19 out of 23 isolated culturable microorganisms were identified by 16S rRNA sequencing (Table 8). The identified microorganisms belonged to *Pseudomonadota*, *Bacillota* and *Actinomycetota*, being consistent with the dominant phyla in other dust studies [9,65,67]. *Pseudomonadota* (nmc = 6) was the predominant phylum in sample M2, followed by *Bacillota* (nmc = 4) and *Actinomycetota* (nmc = 2). On the other hand, sample M3 showed the same proportions in each phylum. Sample M1 was represented by only one microorganism belonging to *Bacillota*, corroborating its low bacterial abundance.

Most of the identified microorganisms had previously been isolated from soil samples, with some of them being described as extremophiles. Bacteria with beneficial effects on plants, such as Plant Growth-Promotion Rhizobacteria (PGPR), were detected in our samples. *Peribacillus frigiditolerans*, isolated for the first time in arid soils from Morocco, is an extremophilic microorganism, involved in soil bioremediation, with a promising PGPR activity [68–70]. *Bacillus safensis* subsp. *safensis* and *Paenarthrobacter nitroguajacolicus* possess PGPR properties that may be potentially viable even in extreme environments due to their tolerance to harsh conditions [71,72]. On the other hand, *Pseudomonas alloputida* and *Pseudomonas humanensis* have PGPR properties and are also efficient in soil bioremediation [73,74]. *Pseudomonas humanensis* and *Peribacillus frigiditolerans* were previously isolated in samples of Sahara dust plumes deposited as red rain in the southeast of Spain [16].

Plant and animal pathogens were found among the identified species. *Pantoea endophytica* has recently been described as a plant pathogen, causing bacterial rot in tobacco plantations [75]. *Sanguibacter inulinus* and *Sanguibacter keddiei* are potential animal pathogens which were first isolated from blood in apparently healthy cows [76,77].

Bacteria with detrimental effects on human health were also isolated from our samples. *Acinetobacter lwoffii* and *Niallia circulans* are pathogen strains involved in human infections and especially in immunodeficient patients [78,79]. Similarly, *Micrococcus luteus*, *Enterobacter cancerogenus* and *Pseudodescherichia vulneris* are opportunistic pathogens that cause infections in humans [80,81]. Interestingly, *Acinetobacter lwoffii* was also identified in Saharan dust collected in Greece (the eastern Mediterranean) [63].

There is a pressing need for more extensive, long-term studies to elucidate the observed variations in airborne microbial communities worldwide. Given the current scenario of global climate change and the potential impact of microorganisms on recipient ecosystems (such as public health and agronomy), it is essential to foster new scientific advancements and collaborative alliances. This will enable us to investigate the transport and viability of specific microbes through diverse atmospheric routes and evaluate their persistence over time.

## 5. Conclusions and Closing Remarks

The Canary Islands are frequently affected by Saharan dust intrusions, owing to their proximity to North Africa, making them an ideal location for atmospheric dust sampling. Culturable microorganisms and their mineral–bacteria interactions were studied for the first time in Saharan dust collected during three calima events (2021–2022) in Gran Canary Island (close to Morocco). Iberulites—a singular type of giant quasi-spherical particle generated in the troposphere, with a diameter between 50 and 200  $\mu\text{m}$ —were identified during the events. Bacterial colonies and biofilm were observed in the mineral particle surfaces and in the iberulites. The atmospheric dust constitutes an authentic medium for bacterial growth, a novel finding evinced in the SEM images.

For the first time, a process of neof ormation of nanometric kaolinite crystals mediated by microorganisms has been described in the atmosphere, which has been limited to laboratory studies until now.

Twenty-three culturable microorganisms were isolated and identified by 16S rRNA sequencing. Members of the phyla *Pseudomonadota*, *Bacillota* and *Actinomycetota* have been

found. Some species have shown beneficial effects in plants (*Peribacillus frigoritolerans*), whereas others are potential pathogens for human health (*Acinetobacter lwoffii*).

Calimas in the Canary Islands are natural phenomena, which are not controllable, nor is it possible to reduce them. The prevention and control of these phenomena should be approached from the novel and holistic perspective of “One Health”, which recognises that human health is closely linked to animal and environmental health. Our work can contribute to a better understanding of their effects on the population and ecosystems. Many new microbiomes undoubtedly await description, such as the aerobiome, and its emerging study may represent one of the major challenges of the future.

**Author Contributions:** Methodology, A.d.M., R.D. and J.P.; software, A.N., J.M.M.-G. and F.M.-C.; formal analysis, A.N., I.d.P. and F.M.-C.; investigation, A.N., A.d.M., R.D., J.P., J.M.M.-G. and F.M.-C.; data curation, A.d.M., R.D., J.P., J.M.M.-G. and F.M.-C.; writing—original draft, A.N., A.d.M., R.D. and J.P.; visualization, J.M.M.-G. All authors have read and agreed to the published version of the manuscript.

**Funding:** This research received no external funding.

**Institutional Review Board Statement:** Not applicable.

**Informed Consent Statement:** Not applicable.

**Data Availability Statement:** Data are contained within the article.

**Acknowledgments:** The authors gratefully acknowledge the NOAA Air Resources Laboratory (ARL) for the provision of the HYSPLIT transport and dispersion model and the READY website (<https://www.ready.noaa.gov> (accessed on 7 May 2022)) used in this publication. Dust surface concentration images were provided by the WMO Barcelona Dust Regional Center and the partners of the Sand and Dust Storm Warning Advisory and Assessment System (SDS-WAS) for Northern Africa, the Middle East and Europe.

**Conflicts of Interest:** The authors declare no conflicts of interest.

## References

- Rodríguez-Arias, R.M.; Rojo, J.; Fernández-González, F.; Pérez-Badia, R. Desert dust intrusions and their incidence on airborne biological content. review and case study in the Iberian peninsula. *Environ. Pollut.* **2023**, *316*, 120464. [CrossRef]
- Zender, C.S.; Miller, R.L.; Tegen, I. Quantifying mineral dust mass budgets: Terminology, constraints, and current estimates. *Eos Trans. Am. Geophys. Union* **2004**, *85*, 509–512. [CrossRef]
- Goudie, A.; Middleton, N. Desert dust in the global system. In *Desert Dust in the Global System*; Springer Science & Business Media: Berlin, Germany, 2006; pp. 1–287. [CrossRef]
- Shao, Y.; Wyrwoll, K.H.; Chappell, A.; Huang, J.; Lin, Z.; McTainsh, G.H.; Mikami, M.; Tanaka, T.Y.; Wang, X.; Yoon, S. Dust Cycle: An emerging core theme in earth system science. *Aeolian Res.* **2011**, *2*, 181–204. [CrossRef]
- Shu, W.S.; Huang, L.N. Microbial diversity in extreme environments. *Nat. Rev. Microbiol.* **2022**, *20*, 219–235. [CrossRef] [PubMed]
- Péguilhan, R.; Rossi, F.; Rué, O.; Joly, M.; Amato, P. Comparative Analysis of Bacterial Diversity in Clouds and Aerosols. *Atmos. Environ.* **2023**, *298*, 119635. [CrossRef]
- Rahav, E.; Paytan, A.; Mesciöglu, E.; Bar-Zeev, E.; Ruiz, F.M.; Xian, P.; Herut, B. Bio-aerosols negatively affect *Prochlorococcus* in oligotrophic aerosol-rich marine regions. *Atmosphere* **2020**, *11*, 540. [CrossRef]
- Varga, G.; Knippertz, P.; Stuut, J.-B.W. (Eds.) Mineral dust—A key player in the earth system. *Hung. Geogr. Bull.* **2016**, *65*, 84–85. [CrossRef]
- Federici, E.; Petroselli, C.; Montalbani, E.; Casagrande, C.; Ceci, E.; Moroni, B.; La Porta, G.; Castellini, S.; Selvaggi, R.; Sebastiani, B.; et al. Airborne bacteria and persistent organic pollutants associated with an intense Saharan dust event in the central Mediterranean. *Sci. Total Environ.* **2018**, *645*, 401–410. [CrossRef]
- Gat, D.; Zimmermann, R.; Rudich, Y. Functional genes profile of atmospheric dust in the east Mediterranean suggests widespread anthropogenic influence on aerobiome composition. *J. Geophys. Res. Biogeosci.* **2022**, *127*, e2022JG007022. [CrossRef]
- González-Toril, E.; Osuna, S.; Viúdez-Moreiras, D.; Navarro-Cid, I.; Toro, S.D.d.; Sor, S.; Bardera, R.; Puente-Sánchez, F.; de Diego-Castilla, G.; Aguilera, Á. Impacts of Saharan dust intrusions on bacterial communities of the low troposphere. *Sci. Rep.* **2020**, *10*, 6837. [CrossRef]
- Sánchez De La Campa, A.; García-Salamanca, A.; Solano, J.; De La Rosa, J.; Ramos, J.L. Chemical and microbiological characterization of atmospheric particulate matter during an intense African dust event in southern Spain. *Environ. Sci. Technol.* **2013**, *47*, 3630–3638. [CrossRef]

13. Barton, A.D.; Dutkiewicz, S.; Flierl, G.; Bragg, J.; Follows, M.J. Patterns of diversity in marine phytoplankton. *Science* **2010**, *327*, 1509–1511. [[CrossRef](#)]
14. Avila, A.; Peñuelas, J. Increasing frequency of Saharan rains over northeastern Spain and its ecological consequences. *Sci. Total Environ.* **1999**, *228*, 153–156. [[CrossRef](#)]
15. Fiol, L.A.; Fornós, J.J.; Gelabert, B.; Guijarro, J.A. Dust rains in Mallorca (western Mediterranean): Their occurrence and role in some recent geological processes. *Catena* **2005**, *63*, 64–84. [[CrossRef](#)]
16. Navarro, A.; del Moral, A.; Weber, B.; Weber, J.; Molinero, A.; Delgado, R.; Párraga, J.; Martínez-Checa, F. Microbial composition of Saharan dust plumes deposited as red rain in Granada (southern Spain). *Sci. Total Environ.* **2024**, *913*, 169745. [[CrossRef](#)]
17. Díaz-Hernández, J.L.; Párraga, J. The nature and tropospheric formation of iberulites: Pinkish mineral microspherulites. *Geochim. Cosmochim. Acta* **2008**, *72*, 3883–3906. [[CrossRef](#)]
18. Párraga, J.; Martín-García, J.M.; Delgado, G.; Molinero-García, J.A.; Cervera-Mata, A.I.; Guerra, J.A.; Fernández-González, M.V.; Martín-Rodríguez, J.M.; Lyamani, H.; Casquero-Vera, J.A.; et al. Intrusions of dust and iberulites in Granada basin (southern Iberian Peninsula). genesis and formation of atmospheric iberulites. *Atmos. Res.* **2021**, *248*, 105260. [[CrossRef](#)]
19. Menéndez, I.; Díaz-Hernández, J.L.; Mangas, J.; Alonso, I.; Sánchez-Soto, P.J. Airborne dust accumulation and soil development in the north-east sector of Gran Canaria (Canary Islands, Spain). *J. Arid. Environ.* **2007**, *71*, 57–81. [[CrossRef](#)]
20. Villarrubia, L.; García Pérez, M.D.; Petral, N.; Ballester, F.; Iñiguez, C.; Pita, M.L. Caracterización del ambiente atmosférico de Las Palmas de Gran Canaria y Santa Cruz de Tenerife. *Rev. Esp. Salud Pública* **2008**, *82*, 439–508.
21. Menéndez, I.; Derbyshire, E.; Engelbrecht, J.; von Suchodoletz, H.; Zoeller, L.; Dorta Antequera, P.; Carrillo, T.; Castro, F.C.B.R. De Saharan dust and the aerosols on the Canary Islands: Past and present. *Airborne Part.* **2009**, 39–80.
22. Dorta, P.; Gelado, M.D.; Hernández, J.J.; Cardona, P.; Collado, C.; Mendoza, S.; Rodríguez, M.J.; Siruela, V.; Torres, M.E. Frecuencia, estacionalidad y tendencias de las advecciones de aire sahariano en Canarias (1976–2003). *Investig. Geográficas (Esp)* **2005**, *38*, 23–45. [[CrossRef](#)]
23. Ministry for Ecological Transition and Demographic Challenge. Histórico de Informes de Episodios Naturales. 2021. Available online: <https://www.miteco.gob.es/es/calidad-y-evaluacion-ambiental/temas/atmosfera-y-calidad-del-aire/calidad-del-aire/evaluacion-datos/fuentes-naturales/anuales.aspx> (accessed on 25 January 2024). (In Spanish)
24. Ministry for Ecological Transition and Demographic Challenge. Histórico de Informes de Episodios Naturales. 2022. Available online: <https://www.miteco.gob.es/es/calidad-y-evaluacion-ambiental/temas/atmosfera-y-calidad-del-aire/calidad-del-aire/evaluacion-datos/fuentes-naturales/anuales.aspx> (accessed on 25 January 2024). (In Spanish)
25. Pérez, C.; Haustein, K.; Janjic, Z.; Jorba, O.; Huneeus, N.; Baldasano, J.M.; Black, T.; Basart, S.; Nickovic, S.; Miller, R.L.; et al. Atmospheric dust modeling from meso to global scales with the online NMMB/BSC-Dust Model &ndash; Part 1: Model Description, Annual Simulations and Evaluation. *Atmos. Chem. Phys.* **2011**, *11*, 13001–13027. [[CrossRef](#)]
26. Klose, M.; Jorba, O.; Gonçalves Ageitos, M.; Escribano, J.; Dawson, M.L.; Obiso, V.; Di Tomaso, E.; Basart, S.; Montané Pinto, G.; Macchia, F.; et al. Mineral dust cycle in the multiscale online nonhydrostatic atmosphere chemistry model (MONARCH) Version 2.0. *Geosci. Model. Dev.* **2021**, *14*, 6403–6444. [[CrossRef](#)]
27. Draxler, R.R.; Rolph, G.D. HYSPLIT (HYbrid Single-Particle Lagrangian Integrated Trajectory) Model Acces Via. NOAA ARL RADY Website. 2015. Available online: <https://www.ready.noaa.gov/HYSPLIT.php> (accessed on 7 May 2022).
28. Gobierno de Canarias Red de Vigilancia de la Calidad del aire de Canarias. Hourly and Daily Quality Reports. Available online: <https://www3.gobiernodecanarias.org/medioambiente/calidaddelaire/datosHistoricosForm.do> (accessed on 30 January 2024).
29. Martín-Ramos, J.D. X Powder, a Software Package for Powder X-ray Diffraction Analysis. 2004. Available online: <http://www.xpowder.com> (accessed on 21 June 2022).
30. Schultz, L.G. Quantitative interpretation of mineralogical composition from X-ray and chemical data for the pierre shale. *US Geol. Surv. Prof. Pap.* **1964**, *391C*, 31.
31. Delgado, R.; Barahona, E.; Huertas, F.; Linares, J. Los mollisoles de la cuenca alta del río Dílar (Sierra Nevada). *An. De Edafol. Y Agrobiol.* **1982**, *41*, 59–82.
32. Barahona, E. Arcillas de Ladrillería de la Provincia de Granada: Evaluación de Algunos Ensayos de Materias Primas. Doctoral Thesis, Universidad de Granada, Granada, Spain, 1974.
33. Kuo, J. Electron microscopy methods and protocols Third Edition Preface. In *Electron Microscopy: Methods and Protocols*; Kuo, J., Ed.; Methods in Molecular Biology; Springer Science & Business Media: Berlin, Germany, 2014; Volume 1117, pp. VII–VIII. ISBN 978-1-62703-776-1.
34. Altschul, S.F.; Gish, W.; Miller, W.; Myers, E.W.; Lipman, D.J. Basic local alignment search tool. *J. Mol. Biol.* **1990**, *215*, 403–410. [[CrossRef](#)]
35. Yoon, S.H.; Ha, S.M.; Kwon, S.; Lim, J.; Kim, Y.; Seo, H.; Chun, J. Introducing EzBioCloud: A taxonomically united database of 16S rRNA gene sequences and whole-genome assemblies. *Int. J. Syst. Evol. Microbiol.* **2017**, *67*, 1613–1617. [[CrossRef](#)] [[PubMed](#)]
36. Rodríguez, S.; Cuevas, E.; Prospero, J.M.; Alastuey, A.; Querol, X.; López-Solano, J.; García, M.I.; Alonso-Pérez, S. Modulation of Saharan dust export by the north African dipole. *Atmos. Chem. Phys.* **2015**, *15*, 7471–7486. [[CrossRef](#)]
37. Menéndez, I.; Pérez-Chacón, E.; Mangas, J.; Tauler, E.; Engelbrecht, J.P.; Derbyshire, E.; Cana, L.; Alonso, I. Dust Deposits on La Graciosa Island (Canary Islands, Spain): Texture, mineralogy and a case study of recent dust plume transport. *Catena* **2014**, *117*, 133–144. [[CrossRef](#)]

38. Criado, C.; Dorta, P. An unusual “blood rain” over the Canary Islands (Spain). The storm of January 1999. *J. Arid. Environ.* **2003**, *55*, 765–783. [[CrossRef](#)]
39. Littman, T. Rainfall, temperature and dust storm anomalies in the African Sahel. *Geogr. J.* **1991**, *157*, 136–160. [[CrossRef](#)]
40. Jeong, G.Y.; Park, M.Y.; Kandler, K.; Nousiainen, T.; Kemppinen, O. Mineralogical properties and internal structures of individual fine of Saharan dust. *Atmos. Chem. Phys.* **2016**, *16*, 12397–12410. [[CrossRef](#)]
41. Avila, A.; Queralt-Mitjans, I.; Alarcón, M. Mineralogical composition of African dust delivered by red rains over northeastern Spain. *J. Geophys. Res. Atmos.* **1997**, *102*, 21977–21996. [[CrossRef](#)]
42. Scheuven, D.; Schütz, L.; Kandler, K.; Ebert, M.; Weinbruch, S. Bulk composition of northern African dust and its source sediments—A compilation. *Earth Sci. Rev.* **2013**, *116*, 170–194. [[CrossRef](#)]
43. Claquin, T.; Schulz, M.; Balkanski, Y.J. Modeling the mineralogy of atmospheric dust sources. *J. Geophys. Res. Atmos.* **1999**, *104*, 22243–22256. [[CrossRef](#)]
44. Lafon, S.; Rajot, J.; Alfaro, S.; Gaudichet, A. Quantification of iron oxides in desert aerosol. *Atmos. Environ.* **2004**, *38*, 1211–1218. [[CrossRef](#)]
45. Eswaran, H.; Zi-Tong, G. Properties, genesis, classification, and distribution of soils with gypsum. In *Occurrence, Characteristics, and Genesis of Carbonate, Gypsum, and Silica Accumulations in Soils*; John Wiley & Sons, Ltd.: Hoboken, NJ, USA, 1991; pp. 89–119. ISBN 9780891189213.
46. Wagner, C.D.; Naumkin, A.V.; Kraut-Vass, A.; Allison, J.W.; Powell, C.J.; Rumble, J.R., Jr. NIST Standard Reference Database 20, version 3.4. Available online: <http://srdata.nist.gov/xps/> (accessed on 30 January 2024).
47. Seyama, H.; Soma, M. X-ray Photoelectron Spectroscopic Study of Montmorillonite Containing Exchangeable Divalent Cations. *J. Chem. Soc. Faraday Trans. 1 Phys. Chem. Condens. Phases* **1984**, *80*, 237–248. [[CrossRef](#)]
48. Gerin, P.A.; Dufrière, Y.F. Native surface structure of natural soil particles determined by combining atomic force microscopy and X-ray photoelectron spectroscopy. *Colloids Surf. B Biointerfaces* **2003**, *28*, 295–305. [[CrossRef](#)]
49. Biesinger, M.C.; Payne, B.P.; Grosvenor, A.P.; Lau, L.W.M.; Gerson, A.R.; Smart, R.S.C. Resolving surface chemical states in XPS analysis of first row transition metals, oxides and hydroxides: Cr, Mn, Fe, Co and Ni. *Appl. Surf. Sci.* **2011**, *257*, 2717–2730. [[CrossRef](#)]
50. Flogéac, K.; Guillon, E.; Aplincourt, M.; Marceau, E.; Stievano, L.; Beaunier, P.; Frapart, Y.M. Characterization of soil particles by X-ray diffraction (XRD), X-ray photoelectron spectroscopy (XPS), electron paramagnetic resonance (EPR) and transmission electron microscopy (TEM). *Agron. Sustain. Dev.* **2005**, *25*, 345–353. [[CrossRef](#)]
51. Stipp, S.L.; Hochella, M.F. Structure and bonding environments at the calcite surface as observed with X-ray photoelectron spectroscopy (XPS) and low energy electron diffraction (LEED). *Geochim. Cosmochim. Acta* **1991**, *55*, 1723–1736. [[CrossRef](#)]
52. Wren, A.G.; Phillips, R.W.; Tolentino, L.U. Surface reactions of chlorine molecules and atoms with water and sulfuric acid at low temperatures. *J. Colloid. Interface Sci.* **1979**, *70*, 544–557. [[CrossRef](#)]
53. Wagner, C.; Fournier, N.; Tautz, F.S.; Temirov, R. Measurement of the Binding Energies of the Organic-Metal Perylene-Teracarboxylic-Dianhydride/Au(111) Bonds by molecular manipulation using an atomic force microscope. *Phys. Rev. Lett.* **2012**, *109*, 076102. [[CrossRef](#)]
54. Alastuey, A.; Querol, X.; Castillo, S.; Escudero, M.; Avila, A.; Cuevas, E.; Torres, C.; Romero, P.-M.; Exposito, F.; García, O.; et al. Characterisation of TSP and PM<sub>2.5</sub> at Izaña and Sta. Cruz de Tenerife (Canary Islands, Spain) during a Saharan Dust Episode (July 2002). *Atmos. Environ.* **2005**, *39*, 4715–4728. [[CrossRef](#)]
55. Biesinger, M.C.; Lau, L.W.M.; Gerson, A.R.; Smart, R.S.C. Resolving surface chemical states in XPS analysis of first row transition metals, oxides and hydroxides: Sc, Ti, V, Cu and Zn. *Appl. Surf. Sci.* **2010**, *257*, 887–898. [[CrossRef](#)]
56. Querol, X.; Tobías, A.; Pérez, N.; Karanasiou, A.; Amato, F.; Stafoggia, M.; Pérez García-Pando, C.; Ginoux, P.; Forastiere, F.; Gummy, S.; et al. Monitoring the impact of desert dust outbreaks for air quality for health studies. *Environ. Int.* **2019**, *130*, 104867. [[CrossRef](#)]
57. Favet, J.; Lapanje, A.; Giongo, A.; Kennedy, S.; Aung, Y.Y.; Cattaneo, A.; Davis-Richardson, A.G.; Brown, C.T.; Kort, R.; Brumsack, H.J.; et al. Microbial hitchhikers on intercontinental dust: Catching a lift in Chad. *ISME J.* **2013**, *7*, 850–867. [[CrossRef](#)]
58. Šantl-Temkiv, T.; Amato, P.; Casamayor, E.O.; Lee, P.K.H.; Pointing, S.B. Microbial ecology of the atmosphere. *FEMS Microbiol. Rev.* **2022**, *46*, fuac009. [[CrossRef](#)]
59. Linares, J.; Huertas, F. Kaolinite: Synthesis at room temperature. *Science* **1971**, *171*, 896–897. [[CrossRef](#)]
60. Párraga, J.; Rivadeneyra, M.A.; Martín-García, J.M.; Delgado, R.; Delgado, G. Precipitation of carbonates by bacteria from a saline soil, in natural and artificial soil extracts. *Geomicrobiol. J.* **2004**, *21*, 55–66. [[CrossRef](#)]
61. Fiore, S.; Dumontet, S.; Huertas, F.J.; Pasquale, V. Bacteria-induced crystallization of kaolinite. *Appl. Clay Sci.* **2011**, *53*, 566–571. [[CrossRef](#)]
62. Bontognali, T.R.R.; Martínez-Ruiz, F.; McKenzie, J.A.; Bahniuk, A.; Anjos, S.; Vasconcelos, C. Smectite synthesis at low temperature and neutral pH in the presence of succinic acid. *Appl. Clay Sci.* **2014**, *101*, 553–557. [[CrossRef](#)]
63. Polymenakou, P.N.; Mandalakis, M.; Stephanou, E.G.; Tselepidis, A. Particle size distribution of airborne microorganisms and pathogens during an intense African dust event in the eastern mediterranean. *Environ. Health Perspect.* **2008**, *116*, 292–296. [[CrossRef](#)]
64. Hara, K.; Zhang, D. Bacterial abundance and viability in long-range transported dust. *Atmos. Environ.* **2012**, *47*, 20–25. [[CrossRef](#)]



65. Stern, R.A.; Mahmoudi, N.; Buckee, C.O.; Schartup, A.T.; Koutrakis, P.; Ferguson, S.T.; Wolfson, J.M.; Wofsy, S.C.; Daube, B.C.; Sunderland, E.M. The microbiome of size-fractionated airborne particles from the Sahara region. *Environ. Sci. Technol.* **2021**, *55*, 1487–1496. [[CrossRef](#)] [[PubMed](#)]
66. Hoffmann, T.D.; Reeksting, B.J.; Gebhard, S. Bacteria-induced mineral precipitation: A mechanistic review. *Microbiology* **2021**, *167*, 001049. [[CrossRef](#)] [[PubMed](#)]
67. Das, S.; McEwen, A.; Prospero, J.; Spalink, D.; Chellam, S. Respirable metals, bacteria, and fungi during a Saharan–Sahelian dust event in Houston, Texas. *Environ. Sci. Technol.* **2023**, *57*, 19942–19955. [[CrossRef](#)] [[PubMed](#)]
68. Marik, D.; Sharma, P.; Singh Chauhan, N.; Jangir, N.; Singh Shekhawat, R.; Verma, D.; Mukherjee, M.; Abiala, M.; Roy, C.; Yadav, P. *Peribacillus frigoritolerans* T7-IIT], a potential biofertilizer, induces plant growth-promoting genes of *Arabidopsis thaliana*. *bioRxiv* **2023**. [[CrossRef](#)]
69. Jariyal, M.; Gupta, V.; Mandal, K.; Jindal, V. *Brevibacterium frigoritolerans* as a novel organism for the bioremediation of phorate. *Bull. Environ. Contam. Toxicol.* **2015**, *95*, 680–686. [[CrossRef](#)] [[PubMed](#)]
70. Świątczak, J.; Kalwasińska, A.; Brzezinska, M.S. Plant growth–promoting rhizobacteria: *Peribacillus frigoritolerans* 2RO30 and *Pseudomonas Sivasensis* 2RO45 for their effect on canola growth under controlled as well as natural conditions. *Front. Plant Sci.* **2023**, *14*, 1233237. [[CrossRef](#)] [[PubMed](#)]
71. Lateef, A.; Adelere, I.A.; Gueguim-Kana, E.B. *Bacillus Safensis* LAU 13: A new source of keratinase and its multi-functional biocatalytic applications. *Biotechnol. Biotechnol. Equip.* **2015**, *29*, 54–63. [[CrossRef](#)]
72. Salimi, F.; Khorshidi, M.; Amirahmadi, F.; Amirahmadi, A. Effectiveness of phosphate and zinc solubilizing *Paenarthrobacter nitroguajacolicus* P1 as *Halotolerant rhizobacterium* with growth-promoting activity on *Pistacia vera* L. *Curr. Microbiol.* **2023**, *80*, 336. [[CrossRef](#)] [[PubMed](#)]
73. Bakaeva, M.; Kuzina, E.; Vysotskaya, L.; Kudoyarova, G.; Arkhipova, T.; Rafikova, G.; Chetverikov, S.; Korshunova, T.; Chetverikova, D.; Loginov, O. Capacity of *Pseudomonas* strains to degrade hydrocarbons, produce auxins and maintain plant growth under normal conditions and in the presence of petroleum contaminants. *Plants* **2020**, *9*, 379. [[CrossRef](#)] [[PubMed](#)]
74. Passarelli-Araujo, H.; Jacobs, S.H.; Franco, G.R.; Venancio, T.M. Phylogenetic analysis and population structure of *Pseudomonas alloputida*. *Genomics* **2021**, *113*, 3762–3773. [[CrossRef](#)] [[PubMed](#)]
75. Ilyas, N.; Yang, Y.; Liu, W.; Li, X.; Pu, W.; Singh, R.P.; Li, Y. First report of bacterial rot caused by *Pantoea endophytica* on tobacco in Liuyang, China. *Plant Dis.* **2021**, *105*, 4147. [[CrossRef](#)] [[PubMed](#)]
76. Ivanova, N.; Sikorski, J.; Sims, D.; Brettin, T.; Detter, J.C.; Han, C.; Lapidus, A.; Copeland, A.; Glavina, T.; Rio, D.; et al. Complete genome sequence of *Sanguibacter keddieii* type strain (ST-74 T). *Stand. Genomic Sci.* **2009**, *1*, 110–118. [[CrossRef](#)] [[PubMed](#)]
77. Pascual, C.; Collins, M.D.; Grimont, P.A.D.; Domínguez, L.; Fernández-Garayzabal, J.F. NOTES: *Sanguibacter inulinus* Sp. Nov. *Int. J. Syst. Evol. Microbiol.* **1996**, *46*, 811–813. [[CrossRef](#)] [[PubMed](#)]
78. Orimi, G.P.; Sherafat, J.S.; Mojarad, N.E. Fatal Sepsis by *Bacillus circulans* in an immunocompromised patient. *Iran. J. Microbiol.* **2011**, *3*, 156.
79. Ku, S.C.; Hsueh, P.R.; Yang, P.C.; Luh, K.T. *Clinical and Microbiological Characteristics of Bacteremia Caused by Acinetobacter Lwoffii*; Springer: Berlin, Germany, 2000; Volume 19.
80. Demir, T.; Baran, G.; Buyukguclu, T.; Sezgin, F.M.; Kaymaz, H. Pneumonia due to *Enterobacter cancerogenus* infection. *Folia Microbiol.* **2014**, *59*, 527–530. [[CrossRef](#)]
81. Jain, S.; Nagarjuna, D.; Gaiind, R.; Chopra, S.; Debata, P.K.; Dawar, R.; Sardana, R.; Yadav, M. *Escherichia vulneris*: An unusual cause of complicated diarrhoea and sepsis in an infant. a case report and review of literature. *New Microbes. New Infect.* **2016**, *13*, 83–86. [[CrossRef](#)]

**Disclaimer/Publisher’s Note:** The statements, opinions and data contained in all publications are solely those of the individual author(s) and contributor(s) and not of MDPI and/or the editor(s). MDPI and/or the editor(s) disclaim responsibility for any injury to people or property resulting from any ideas, methods, instructions or products referred to in the content.